

## Multi-layer graphene Pirani pressure sensors

Romijn, J.; Dolleman, R.J.; Singh, M.; van der Zant, H.S.J.; Steeneken, P.G.; Sarro, P.M.; Vollebregt, S.

**DOI**

[10.1088/1361-6528/abff8e](https://doi.org/10.1088/1361-6528/abff8e)

**Publication date**

2021

**Document Version**

Final published version

**Published in**

Nanotechnology

**Citation (APA)**

Romijn, J., Dolleman, R. J., Singh, M., van der Zant, H. S. J., Steeneken, P. G., Sarro, P. M., & Vollebregt, S. (2021). Multi-layer graphene Pirani pressure sensors. *Nanotechnology*, 32(33), Article 335501. <https://doi.org/10.1088/1361-6528/abff8e>

**Important note**

To cite this publication, please use the final published version (if applicable). Please check the document version above.

**Copyright**

Other than for strictly personal use, it is not permitted to download, forward or distribute the text or part of it, without the consent of the author(s) and/or copyright holder(s), unless the work is under an open content license such as Creative Commons.

**Takedown policy**

Please contact us and provide details if you believe this document breaches copyrights. We will remove access to the work immediately and investigate your claim.

PAPER • OPEN ACCESS

## Multi-layer graphene pirani pressure sensors

To cite this article: Joost Romijn *et al* 2021 *Nanotechnology* **32** 335501

View the [article online](#) for updates and enhancements.



**RM5**  
Our confocal  
Raman Microscope.

Your Research. Our Expertise.

EDINBURGH  
INSTRUMENTS

edinst.com

# Multi-layer graphene pirani pressure sensors

Joost Romijn<sup>1</sup> , Robin J Dolleman<sup>2</sup> , Manvika Singh<sup>1</sup>,  
Herre S J van der Zant<sup>3</sup>, Peter G Steeneken<sup>3,4</sup> , Pasqualina M Sarro<sup>1</sup>  and  
Sten Vollebregt<sup>1</sup> 

<sup>1</sup>Laboratory of Electronic Components, Technology and Materials (ECTM), Department of Microelectronics, Delft University of Technology, The Netherlands

<sup>2</sup>Second Institute of Physics, RWTH Aachen University, Germany

<sup>3</sup>Kavli Institute of Nanoscience, Department of Quantum Nanoscience, Delft University of Technology, The Netherlands

<sup>4</sup>Department of Precision and Microsystems Engineering (PME), Delft University of Technology, The Netherlands

E-mail: [J.Romijn@tudelft.nl](mailto:J.Romijn@tudelft.nl)

Received 3 February 2021, revised 2 May 2021

Accepted for publication 10 May 2021

Published 25 May 2021



CrossMark

## Abstract

The operating principle of Pirani pressure sensors is based on the pressure dependence of a suspended strip's electrical conductivity, caused by the thermal conductance of the surrounding gas which changes the Joule heating of the strip. To realize such sensors, not only materials with high temperature dependent electrical conductivity are required, but also minimization of the suspended strip dimensions is essential to maximize the responsivity and minimize the power consumption. Due to this, nanomaterials are especially attractive for this application. Here, we demonstrate the use of a multi-layer suspended graphene strip as a Pirani pressure sensor and compare its behavior with existing models. A clear pressure dependence of the strip's electrical resistance is observed, with a maximum relative change of 2.75% between 1 and 1000 mbar and a power consumption of 8.5 mW. The use of graphene enables miniaturization of the device footprint by 100 times compared to state-of-the-art. Moreover, miniaturization allows for lower power consumption and/or higher responsivity and the sensor's nanogap enables operation near atmospheric pressure that can be used in applications such as barometers for altitude measurement. Furthermore, we demonstrate that the sensor response depends on the type of gas molecules, which opens up the way to selective gas sensing applications. Finally, the graphene synthesis technology is compatible with wafer-scale fabrication, potentially enabling future chip-level integration with readout electronics.

Supplementary material for this article is available [online](#)

Keywords: graphene, microelectromechanical systems (MEMS), microsensors, Pirani pressure sensor, pressure sensors, sensor miniaturization

(Some figures may appear in colour only in the online journal)

## 1. Introduction

Pressure sensors, made using microelectromechanical systems (MEMS) technology, are widely used in integrated systems

and as a consequence there is a constant drive for higher responsivity, lower power consumption, extended operating range and reduced footprint. Historically, integrated circuits have scaled down in size, according to Moore's Law, while at the same time increasing computational speed. Nowadays, Moore's Law has developed into the concept of more than Moore, which demands more functionality in integrated solutions [1]. This trend also drives sensor requirements towards better sensitivity, smaller dimensions and lower power.



Original content from this work may be used under the terms of the [Creative Commons Attribution 4.0 licence](#). Any further distribution of this work must maintain attribution to the author(s) and the title of the work, journal citation and DOI.

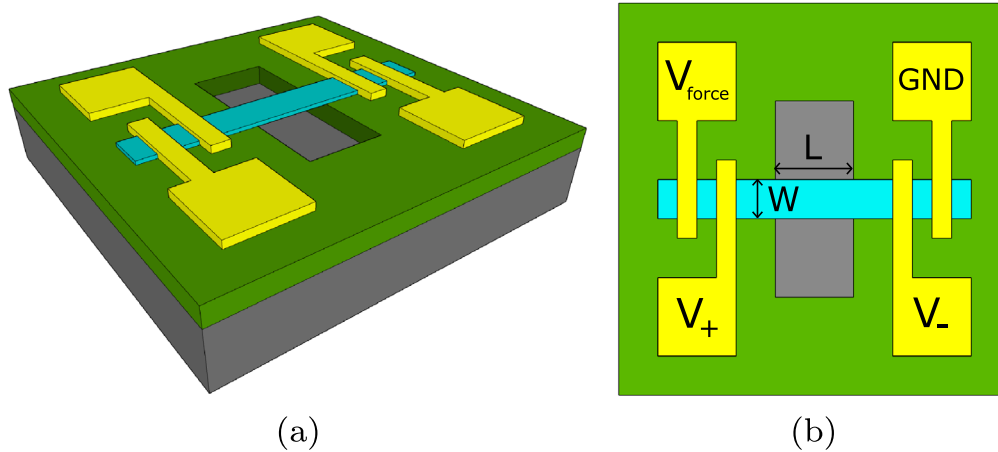


**Figure 1.** Pirani pressure sensor architecture (a) overview and (b) top view. The suspended conductive multi-layer graphene bridge (blue) over a cavity in silicon oxide (green) is the sensing element. Metal traces (yellow) form a structure suitable for 4-point measurements and are marked accordingly.

The Pirani pressure sensor is an often used architecture as it is an attractive design approach for its small size, simplicity, and most importantly robustness, as no moving parts, accurate deflection readout or hermetic cavity are required. The general Pirani architecture is illustrated in figure 1(a), with a top-view in 1(b) indicating the bridge length ( $L$ ) and width ( $W$ ) along with electrical connections for 4-point resistance measurements. The gap size determines the Knudsen's number and therefore the pressure operating range of the device [2] (see supporting information available online at [stacks.iop.org/NANO/32/335501/mmedia](https://stacks.iop.org/NANO/32/335501/mmedia)) and historically, Pirani pressure sensors mostly operate at low pressure conditions. However, tuning the gap size below  $\sim 300$  nm allows operation at ambient pressure [3, 4], enabling a wider range of applications such as barometers for altitude measurements.

The proven analytical Pirani sensor model [2, 5] dictates that the suspended strip's electrical conductivity depends on the Joule heating and the temperature coefficient of resistance (TCR) of the strip material. Within the operation region determined by the gap, the suspended strip's temperature depends on the thermal conductivity of the surrounding gas. The gas temperature is considered constant, leaving the gas composition and pressure as the dominant parameters determining the thermal conductivity of the gas. According to Mastrangelo and Muller [6], the temperature in a Joule heated suspended strip is proportional to the factor  $\delta$ , which is given by

$$\delta = \frac{I_b^2 R_0}{\kappa_b W L t}, \quad (1)$$

where  $I_b$  is the forced electric current through the conductive bridge,  $R_0$  the bridge resistance at ambient temperature and pressure,  $\kappa_b$  the bridge thermal conductivity and  $W$ ,  $L$  and  $t$  the bridge width, length and thickness, respectively. Maximizing  $\delta$ , also maximizes the average temperature increase of the suspended strip, which in turn maximizes the change in electrical resistance. According to equation (1), the factor  $\delta$  is inversely proportional to the suspended strip dimensions. Typical state-of-the-art Pirani implementations

have bridge dimensions of  $100 \mu\text{m} \times 200 \mu\text{m}$  or larger, are thicker than several hundreds of nm and have a power consumption of  $\sim 1$  mW or more [4, 7–12].

Graphene, a single layer sheet of  $sp^2$  bonded carbon atoms, was first isolated in 2004 by Geim and Novoselov using scotch-tape exfoliation from a graphite crystal [13, 14]. It is an extremely attractive material for various types of MEMS devices and sensors [15–17], due to its high mobility [18], large specific surface area and low electric noise [19]. Pressure sensors based on graphene include a squeeze-film [15], piezoresistive [20, 21], osmometer ([22]) and nanodrum [23] pressure sensor. Even multi-layer graphene (MLG) is still orders of magnitude thinner than traditional layers used in state-of-the-art Pirani pressure sensors [4, 7–12]. Therefore, graphene offers tremendous possibilities for miniaturizing the Pirani sensor and at the same time increase its sensitivity. The footprint decrease offers exciting integration possibilities, especially since the graphene synthesis potentially allows integration with CMOS technology on wafer scale [24].

In this work, we demonstrate a graphene-based Pirani pressure sensor that is not only pressure but also gas dependent. Furthermore, we have been able to model the response of the sensor using the analytical Pirani pressure sensor model. The device is highly miniaturized, while retaining sensitivity and power consumption that is comparable with state-of-the-art. The nanogap allows for near atmospheric pressure operation and the selective and the used transfer-free fabrication technology is scalable, enabling future wafer-scale fabrication of the devices.

## 2. Experimental

### 2.1. Device description

The graphene-based Pirani pressure sensor [25] is implemented by a  $\sim 8$  nm suspended MLG strip, that is grown using a selective and transfer-free CVD fabrication method [26]. This method encompasses the sputter deposition of a thin-film

of Mo on top of thermally grown SiO<sub>2</sub> on the target wafer, which is then selectively patterned through dry etching with SF<sub>6</sub> through a photoresist mask. Graphene is then selectively deposited on the Mo catalyst through Ar/H<sub>2</sub>/CH<sub>4</sub> at 1000 °C and 25 mbar in an AIXTRON BlackMagic Pro. The MO catalyst layer is removed after the CVD of graphene in a phosphoric acid solution, with the graphene directly sticking to the SiO<sub>2</sub> below. The cavities are etched into a 600 nm SiO<sub>2</sub> layer on a silicon substrate after graphene growth (figure 2(a)), resulting in a gap of ~600 nm. The graphene is electrically contacted using chromium/gold (Cr/Au), 10/100 nm electrodes, to facilitate 4-point measurement of the electrical resistance (figures 1(a) and 1(b)).

The DC characteristics (see figure 8 in the supporting information) of the graphene strips at different temperatures show excellent linearity, from which the graphene TCR is determined to be  $(-3.6 \pm 0.5) \times 10^{-4} \text{ K}^{-1}$ , which matches literature [27]. The geometry and electrical resistance parameters of the samples used in this work are listed in table 1. Due to fabrication limitations, the metal connections are not implemented directly at the edge of the cavity (as shown in figure 1(b)). As a result, the total resistance of the Pirani gauge is the sum of the resistances of the non-suspended and suspended parts of the graphene bridge, as illustrated in figure 2(b).

## 2.2. Pressure dependent measurements

The electrical resistance of different graphene devices as a function of gas pressure is depicted in figure 3(a), over a pressure range from 10 mbar to atmospheric pressure. The electrical resistance change is normalized by

$$\Delta R(p) = \frac{R(p) - R(0)}{R(0)} \times 100. \quad (2)$$

An upward and downward gas pressure sweep is performed and plotted in figure 3(a). As expected, no pressure dependence is observed for non-suspended strips, while suspended strips display a resistance change as function of the gas pressure. The devices are most responsive close to atmospheric pressure and the maximum measured change in resistance between 10 and 1000 mbar is ~2.75% at a power consumption of 8.5 mW for the highest aspect ratio samples.

Furthermore, the pressure dependence for different gas species is measured. The results of a selection of gas compositions is given in figures 3(b) and 3(c) for the 3x6 A device. The range in which the devices are responsive is similar to figure 3(a), which is expected as it is governed by the device its gap size. Clear variations are observed between the pressure dependent electrical resistance in different gases. For example, where helium gas shows a particularly large resistance change, krypton shows a particularly low resistance change. These differences are attributed to the molar mass, and associated variations in the thermal conductivity of the gases, that affect the temperature of the graphene nanobridge. In the next section we will analyze these differences in more detail.

## 2.3. Gas dependent Pirani response

To get a better insight in the gas dependent measurement in figure 3, the curves are fitted by the before mentioned analytical model for Pirani sensors [5, 6]. The physical approximation of the pressure dependent average temperature increase  $\bar{u}(p)$  is modeled here by

$$\bar{u}(p) = \frac{U^2 L}{4R_0 \kappa_b W t} \frac{1}{a^2 x} \left( 1 - \frac{\tanh(a\sqrt{x})}{a\sqrt{x}} \right), \quad (3)$$

where the known parameters are the bias voltage  $U$ , the bridge length  $L$ , width  $W$ , thickness  $t$  and the resistance at the lowest pressure before starting the sweep  $R_0$ . This leaves an arbitrary pressure data vector  $x$ , fitting parameter  $a$  and the thermal conductivity of the suspended graphene strip  $\kappa_b$ . The pressure dependent average temperature increase is calculated by

$$\bar{u}(p) = \frac{1}{\xi} \left( \frac{R(p)}{R_0} - 1 \right), \quad (4)$$

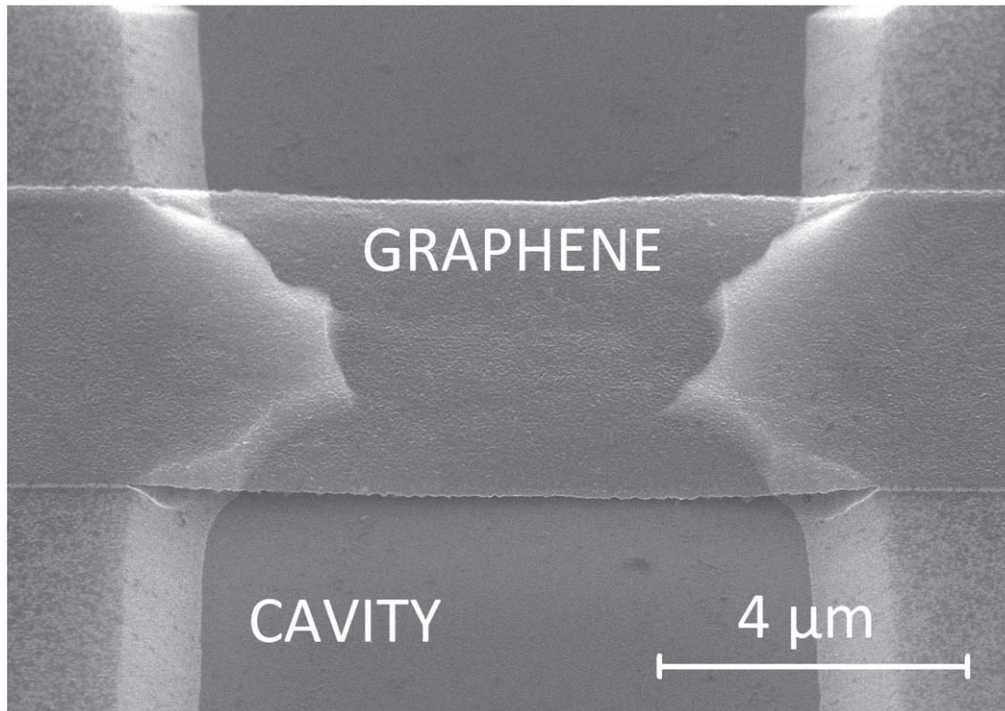
where  $\xi$  is the graphene TCR,  $R(p)$  the pressure dependent measurement of the graphene bridge electrical resistance and  $R_0$  the bridge electrical resistance at low pressure. The fitting results are depicted in figure 4, including the two device geometries and different gases (nitrogen, CO<sub>2</sub>, argon, krypton, air, helium, neon, CF<sub>4</sub>, SF<sub>6</sub> and oxygen). The fit parameters are extracted from the fit, as discussed in the supporting information, which results in a graphene thermal conductivity  $\kappa_b$  in the range of  $2-5 \times 10^3 \text{ W m}^{-1} \text{ K}^{-1}$ . These values are in close correspondence to literature [28].

The results clearly show that the response from the  $2 \times 5 \mu\text{m}$  device is about 2.5 times larger than that of the  $3 \times 6 \mu\text{m}$  device. The different gases result in similar pressure dependency results, though from the responses the different gases can be distinguished. Especially helium, neon and krypton exhibit distinct responses.

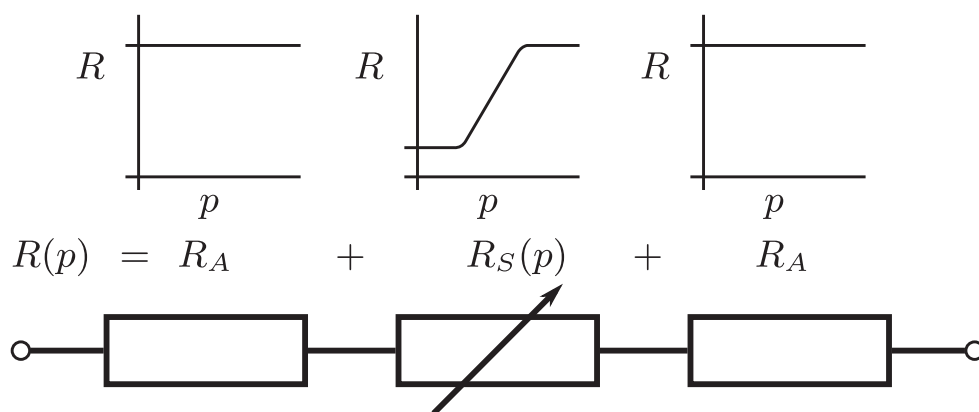
The device's pressure sensitivity is deduced from the fitted curves (see figure 7 in the supporting information) and has maximum sensitivity around 0.6–1 bar. From equation (3) it is deduced that high aspect ratio devices (long and narrow bridges) result in a larger average temperature increase, which implies a higher sensitivity. The maximum values for the sensitivity are ~2.5 %/dec and ~1.1 %/dec for geometries of  $2 \times 5 \mu\text{m}$  and  $3 \times 6 \mu\text{m}$  respectively. In comparison, an overview of reported nano and micro Pirani devices is given in table 2. The maximum sensitivity of krypton, helium and neon deviates from the reported pressure range. This complies with the work of Jousten on the effect of different gases on Pirani gauge readings [29], where corrections for neon and helium were opposite to the correction for krypton.

## 3. Discussion and conclusions

In this work we have demonstrated a nanogap graphene Pirani pressure sensor and studied the effect of pressure, geometry and different gases on the sensor response. Important advantages of the Pirani concept with respect to conventional



(a)



(b)

**Figure 2.** Fabricated graphene-based Pirani pressure sensor (a) and composition (b) of the reported pressure dependent resistance  $R(p)$  including two constant terms  $R_A$  that include the non-suspended graphene strip and a pressure depended suspended strip  $R_S(p)$ .

**Table 1.** The 4-point electrical resistance of the graphene strips used in this study. The total length of all graphene strips is equal. The reported geometries concern only the suspended part of the graphene strip. Samples REF2-3 are non-suspended strips used as reference. Joule heating of the strip was kept to a minimum during the resistance measurement which was performed at atmospheric pressure.

Sample	Strip width	Bridge length	Resistance
2x5 A	2 $\mu\text{m}$	5 $\mu\text{m}$	6.48 k $\Omega$
2x5 B	2 $\mu\text{m}$	5 $\mu\text{m}$	6.57 k $\Omega$
3x6 A	3 $\mu\text{m}$	6 $\mu\text{m}$	5.87 k $\Omega$
3x6 B	3 $\mu\text{m}$	6 $\mu\text{m}$	5.87 k $\Omega$
REF2	2 $\mu\text{m}$	N/A	10.21 k $\Omega$
REF3	3 $\mu\text{m}$	N/A	5.66 k $\Omega$

membrane based pressure sensors are its small size, without moving parts and without the need for a hermetic seal. It is highly miniaturized compared to state-of-the-art implementations, while achieving similar sensitivity values. Furthermore, different gases can be identified by the Pirani sensor, enabling gas sensing applications. The maximum measured sensitivity of the device is  $\sim 2.5\%$ /dec, which is comparable to state-of-the-art Pirani pressure sensors while using a using a 100 times smaller suspended strip area.

The maximum electrical resistance change over the full pressure range that was achieved was 2.75%, which competes with traditional Pirani pressure sensors. For comparison, a negligible pressure dependence of non-suspended graphene strips was observed. The measured response is fitted to an

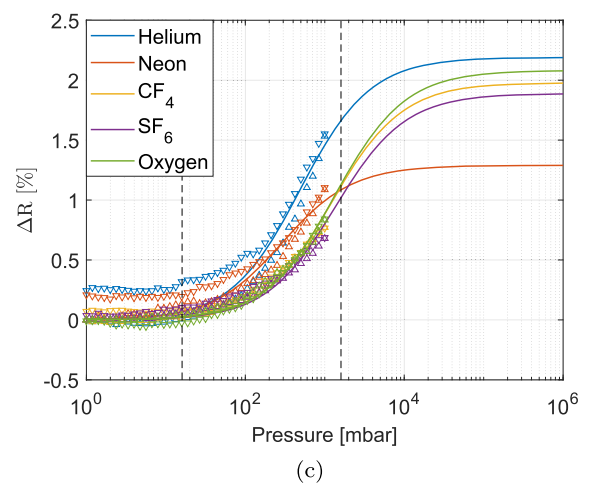
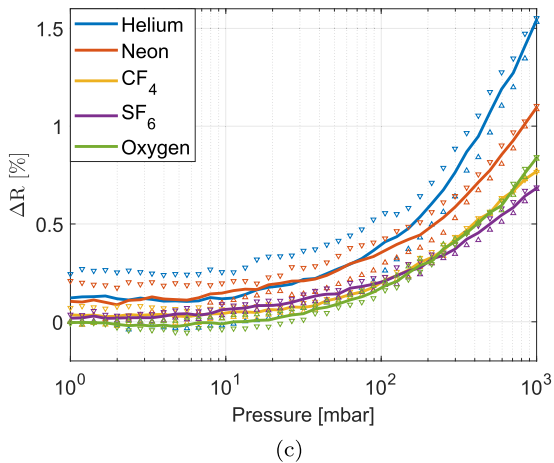
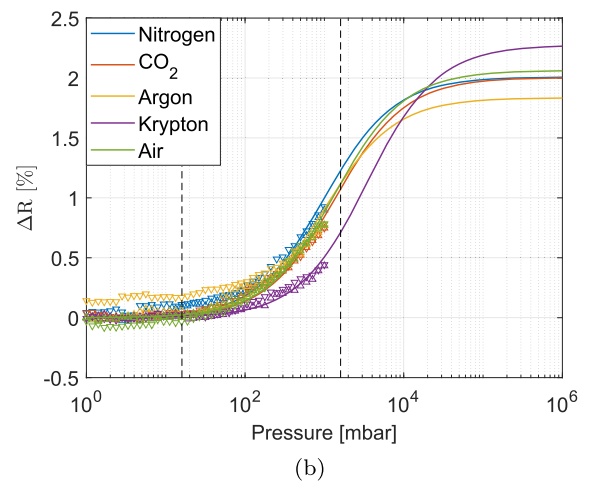
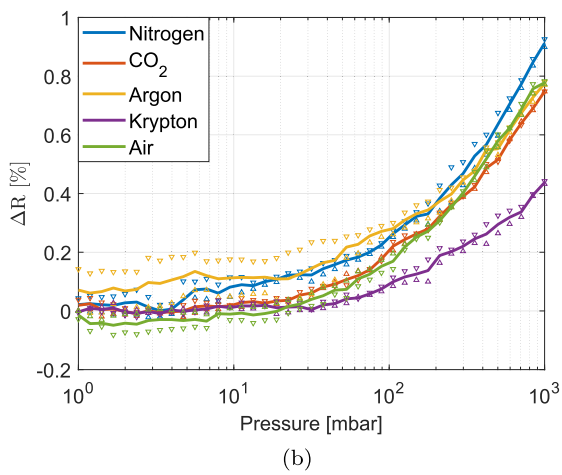
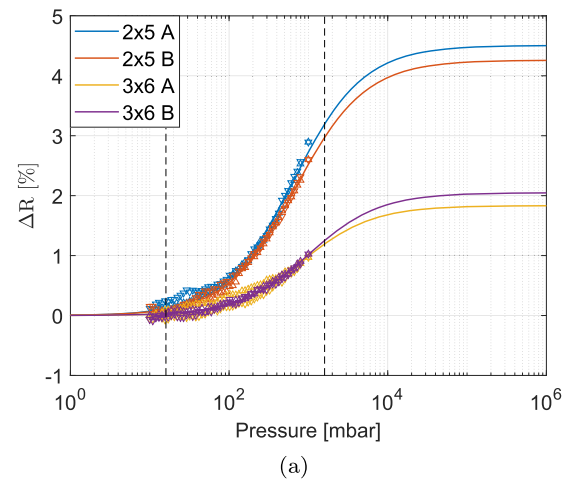
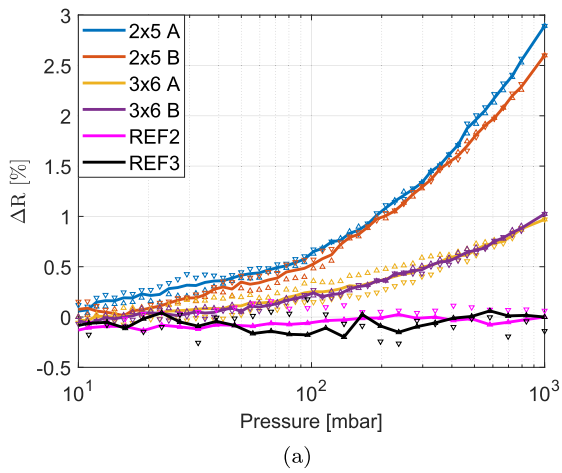


**Figure 3.** Pressure dependence measurement results of the electrical resistance (a) for both suspended and non-suspended graphene strips of different geometries in nitrogen and (b), (c) for different gas species and device 3x6 A. Both upward ‘ $\Delta$ ’ and downward ‘ $\nabla$ ’ pressure sweeps are performed and the average is drawn as a solid line. The resistance  $R_0$  is defined at the lowest pressure in the graph before starting with the upward sweep.

**Figure 4.** Fitting results in extended range showing the full characteristic curve of (a) two device geometries in nitrogen and (b), (c) for different gases and device 3x6 A. Both upward ‘ $\Delta$ ’ and downward ‘ $\nabla$ ’ pressure sweeps are performed and the fit is drawn as a solid line. The resistance  $R_0$  is defined at the lowest pressure in the graph before starting with the upward sweep. The dashed vertical lines project the predicted operating range (supporting information).

**Table 2.** Comparison between previously reported nano and micro Pirani pressure sensors and this work. Note that the reported sensitivities are in the respective device operating ranges, which differ slightly due to differences in the gap size.

Work	Configuration	Sensitivity	Footprint
Puers <i>et al</i> [3]	Quarter-bridge	600 $\mu\text{V}/\text{dec}$	$30 \times 3 \mu\text{m}$
Ghouila-Houri <i>et al</i> [4]	Resistive	36 $\%/ \text{dec}$	$1000 \times 4 \mu\text{m}$
Santagata <i>et al</i> [5]	Resistive	17 $\text{mV}/\text{Pa}^{-1}$	$4 \times 400 \mu\text{m}$
Piotto <i>et al</i> [7]	Resistive	200 $\text{mV}/\text{Pa}^{-1}$	$200 \times 100 \mu\text{m}$
THIS WORK	Resistive	2.5 $\%/ \text{dec}$	$2 \times 5 \mu\text{m}$

analytical model for Pirani pressure sensors. From the fitting results, values for the thermal conductivity of  $2\text{--}5 \times 10^3 \text{ W m}^{-1} \text{ K}^{-1}$  are found, which corresponds well with values reported in literature.

The strong miniaturization, sensitivity at atmospheric pressure, different response for different gases, low-power and potential CMOS integration, allow for exciting future applications. The Pirani sensor can enable applications like system-on-chip (SoC) barometers for altitude measurement and gas identification sensing. To improve the graphene-based Pirani structures, the sensitivity can be improved by reducing the amount of non-suspended graphene that is required for forming electric contacts. Furthermore, the power consumption could further be reduced by implementing lower defect graphene, which typically has a lower sheet resistance. Finally, the fabrication method is scalable, which enables wafer-scale production of the graphene Pirani sensor.

#### 4. Methods

The graphene TCR is obtained from sheet resistance results of non-suspended graphene strips of three different geometries. Wafer-scale measurements were performed on 52 chips in a semi-automatic probe station with the capability of controlling the chuck temperature. The average sheet resistance is obtained for each temperature step, relative to the starting temperature of  $60^\circ\text{C}$ .





The measurement setup [25] used to detect the electrical resistance as function of gas pressure includes a vacuum chamber with mounted sample and electrical feedthroughs connected to the source and measurement unit (Keysight B2901A SMU), which performs 4-point current and voltage measurements on the sample. A Rigol DP832A voltage source pump controller, Proportionair PA2254 dual-valve pressure controller and Keithley 199 pump read-out, connected to a gas source, regulate the pressure inside the chamber. The sample remains equally biased during the chamber pressure adjustments, reducing variations in self-heating of the graphene strip.

#### Acknowledgments

The authors thank the Delft University of Technology Else Kooi Laboratory staff for processing support and the Dutch Technology Foundation (STW), which is part of The

Netherlands Organization for Scientific Research (NWO), and which is partly funded by the Ministry of Economic Affairs, for financially supporting this work under project numbers 13 307 and 13 319 and the European Union's Horizon 2020 research and innovation program under grant agreement number 881 603.

#### ORCID iDs

Joost Romijn  <https://orcid.org/0000-0001-5477-1829>  
 Robin J Dolleman  <https://orcid.org/0000-0002-6976-8443>  
 Peter G Steeneken  <https://orcid.org/0000-0002-5764-1218>  
 Pasqualina M Sarro  <https://orcid.org/0000-0002-2766-0880>  
 Sten Vollebregt  <https://orcid.org/0000-0001-6012-6180>

#### References

- [1] Waldrop M M 2016 The chips are down for Moore's law *Nature* **530** 144–7
- [2] Khosraviani K and Leung A M 2009 The nanogap Pirani—a pressure sensor with superior linearity in an atmospheric pressure range *J. Micromech. Microeng.* **19** 045007
- [3] Puers R, Reyntjens S and Bruyker D D 2002 The NanoPirani—an extremely miniaturized pressure sensor fabricated by focused ion beam rapid prototyping *Sensors Actuators A* **97–98** 208–14
- [4] Ghouila-Houri C, Sindjui R, Moutaouekkil M, Elmazria O, Gallas Q, Garnier E, Merlen A, Viard R, Talbi A and Pernod P 2017 Nanogap Pirani sensor operating in constant temperature mode for near atmospheric pressure measurements *Proc. Eurosens.* **4** 377
- [5] Santagata F, Creemer J F, Iervolino E, Mele L, van Herwaarden A W and Sarro P M 2011 A tube-shaped buried Pirani gauge for low detection limit with small footprint *J. Microelectromech. Syst.* **20** 676–84
- [6] Mastrangelo C H and Muller R S 1991 Microfabricated thermal absolute-pressure sensor with on-chip digital front-end processor *IEEE J. Solid-State Circuits* **26** 1998–2007
- [7] Piotta M, Cesta S D and Bruschi P 2016 A compact CMOS compatible micro-Pirani vacuum sensor with wide operating range and low power consumption *Procedia Eng.* **168** 766–9
- [8] Piotta M, Cesta S D and Bruschi P 2017 A CMOS compatible micro-Pirani vacuum sensor based on mutual heat transfer with 5-decade operating range and 0.3 Pa detection limit *Sensors Actuators A* **263** 718–26
- [9] Claudel J, Ghouila-Houri C, Gerbedoen J-C, Gallas Q, Garnier E, Merlen A, Elmazria O, Viard R, Talbi A and Pernod P 2016 High resolution nano-gap Pirani sensor for pressure measurement in wide dynamic range operation around atmospheric pressure *Procedia Eng.* **168** 798–801



- [10] Sturesson P, Klintberg L and Thornell G 2019 Pirani microgauge fabricated of high-temperature co-fired ceramics with integrated platinum wires *Sensors Actuators A* **285** 8–16
- [11] Jeon G-J, Kim W Y, Shim H B and Lee H C 2016 Nanoporous Pirani sensor based on anodic aluminum oxide *Appl. Phys. Lett.* **109** 123505
- [12] Grau M, Völklein F, Meier A, Kunz C, Kaufmann I and Woias P 2015 Optimized MEMS Pirani sensor with increased pressure measurement sensitivity in the fine and rough vacuum regimes *J. Vac. Sci. Technol. A* **33** 021601
- [13] Novoselov K S, Geim A K, Morozov S V, Jiang D, Katsnelson M I, Grigorieva I V, Dubonos S V and Firsov A A 2005 Two-dimensional gas of massless Dirac fermions in graphene *Nature* **438** 197–200
- [14] Novoselov K S, Geim A K, Morozov S V, Jiang D, Zhang Y, Dubonos S V, Grigorieva I V and Firsov A A 2004 Electric field effect in atomically thin carbon films *Science* **306** 666–9
- [15] Dolleman R J, Davidovikj D, Cartamil-Bueno S J, van der Zant H S J and Steeneken P G 2016a Graphene squeeze-film pressure sensors *Nano Lett.* **16** 568–71
- [16] He Q, Wu S, Yin Z and Zhang H 2012 Graphene-based electronic sensors *Chem. Sci.* **3** 1764–72
- [17] Hill E W, Vijayaraghavan A and Novoselov K 2011 Graphene sensors *IEEE Sensors J.* **11** 3161–70
- [18] Schedin F, Geim A K, Morozov S V, Hill E W, Blake P, Katsnelson M I and Novoselov K S 2007 Detection of individual gas molecules adsorbed on graphene *Nat. Mater.* **6** 652–5
- [19] Balandin A A 2013 Low-frequency  $1/f$  noise in graphene devices *Nat. Nanotechnol.* **8** 549–55
- [20] Smith A D *et al* 2013 Electromechanical piezoresistive sensing in suspended graphene membranes *Nano Lett.* **13** 3237–42
- [21] Zhu S-E, Ghatkesar M K, Zhang C and Janssen G C A M 2013 Graphene based piezoresistive pressure sensor *Appl. Phys. Lett.* **102** 161904
- [22] Dolleman R J, Cartamil-Bueno S J, van der Zant H S J and Steeneken P G 2016b Graphene gas osmometers *2D Mater.* **4** 011002
- [23] Lee M, Davidovikj D, Sajadi B, Šiškins M, Alijani F, van der Zant H S J and Steeneken P G 2019 Sealing graphene nanodrums *Nano Lett.* **19** 5313–8
- [24] Romijn J, Vollebregt S, van Zeijl H W and Sarro P M 2019 A wafer-scale process for the monolithic integration of CVD graphene and CMOS logic for smart MEMS/NEMS sensors *2019 IEEE XXXII Int. Conf. on Micro Electro Mechanical Systems (MEMS)* pp 260–263
- [25] Romijn J, Vollebregt S, Dolleman R J, Singh M, van der Zant H S J, Steeneken P G and Sarro P M 2018 A miniaturized low power Pirani pressure sensor based on suspended graphene *2018 IEEE XIII Annual Int. Conf. on Nano/Micro Engineered and Molecular Systems (NEMS)* pp 11–14
- [26] Vollebregt S, Alfano B, Ricciardella F, Giesbers A J M, Grachova Y, van Zeijl H W, Polichetti T and Sarro P M 2016 A transfer-free wafer-scale CVD graphene fabrication process for MEMS/NEMS sensors *2016 IEEE XXIX Int. Conf. on Micro Electro Mechanical Systems (MEMS)* pp 17–20
- [27] Bae J J, Choi H, Lee Y H and Lim S C 2016 Pressure-dependent heat transfer at multilayer graphene and gas interface *Curr. Appl Phys.* **16** 1236–41 special Section on Nanostructure Physics and Materials Science at Center for Integrated Nanostructure Physics, Institute for Basic Science at Sungkyunkwan University
- [28] Wang N *et al* 2018 Tailoring the thermal and mechanical properties of graphene film by structural engineering *Small* **14** 1801346
- [29] Jousten K 2008 On the gas species dependence of Pirani vacuum gauges *J. Vac. Sci. Technol. A* **26** 352–9